06

Strain sensors based on laser-modified carbon nanostructures for apnea detection

© A.S. Morozova,[1] A.Yu. Gerasimenko[1,2]

[1] Institute of Biomedical Systems, National Research University
„Moscow Institute of Electronic Technology“,
124498 Moscow, Zelenograd, Russia
[2] Institute of Bionic Technologies and Engineering, I.M. Sechenov First Moscow State Medical University,
119991 Moscow, Russia
e-mail: nastya-morozova-2002@list.ru

Received January 8, 2026
Revised January 8, 2026
Accepted January 8, 2026.

The development of carbon nanomaterials such as carbon nanotubes and graphene has made it possible to create flexible strain-sensitive devices for wearable electronics. These devices provide greater efficiency in detecting deformations due to a tight fit to the human body, high elasticity and wearing comfort. In this work flexible strain sensors based on thin films of carbon nanotubes obtained by spray deposition have been developed. The effect of laser radiation on the morphology and electrical characteristics of load cells has been studied. A method for increasing sensitivity using laser lithography to form an electrically conductive topology has been developed. The possibility of monitoring breathing using the developed strain-sensitive sensors has been investigated.

Keywords: strain sensitivity, multi-walled carbon nanotubes, thin films, laser radiation, lithography, respiratory monitoring

DOI: 10.61011/TP.2026.05.63521.337-25

Introduction

Flexible strain gauges are devices capable of reproducing the skin mechanical and sensory functions by combining the know-how in materials science, micro- and nanostructuring, and as well as design of soft electronic systems [1,2]. Biological tissues serve as a guidemark for the development of soft, stretchable and conformal structures that ensure reliable attachment of sensors to the surface of the body during its movement. Along with that, the stringent requirements for sensitivity, linearity, low hysteresis, and speed dictate the need for the formation of multifunctional flexible sensor systems capable of detecting pressure, strain, temperature, and humidity. Due to the combination of low thickness, high stretchability and mobility, such strain-sensitive devices are significantly superior to traditional rigid devices and are used in prosthetics, soft robotics and monitoring of physiological parameters [3–5].

In order to achieve the required mechanical and electrical characteristics, new strategies for the synthesis of flexible materials [6–9] and the design of stretchable and highly sensitive structures [10–14] are being actively explored. However, existing solutions are still limited by a number of factors. The main one is that optimizing one parameter of a strain gauge usually makes the rest ones compromised: e.g., reducing the modulus of elasticity raises the sensitivity, but increases hysteresis [15], reducing the thickness of the dielectric raises the sensitivity, but results in lower durability of the device [16]. Modern research is aimed at solving these problems through the integrated design of materials, structures and interfaces, including the coordinated improvement of mechanical, electrical and morphological parameters at all levels, from nanostructures of active layers to the system integration of multicomponent sensor platforms. This method is formed owing to a slew of accumulated data on the key challenges encountered in the flexible sensors area, including the need to reduce the impact of residual deformations during multiple load cycles, stabilize the response during long-term operation, improve the accuracy of detecting weak mechanical signals, and develop scalable manufacturing methods for highly sensitive systems. Special focus is made on creating materials with predictable deformation behavior, structural solutions that compensate for stretching and twisting, as well as interfaces that ensure reliable contact between soft and hard components. At the same time, strategic growth priorities are being shaped — increasing functional integration, expanding sensor capabilities and developing designs that allow industrial scaling without loss of sensitivity and durability [17–20]. For flexible strain gauges, the mechanical properties of substrates and active materials are of particular importance, since the devices shall maintain the stability of electrical characteristics during stretching, bending and twisting. For example, polymers such as polydimethylsiloxane (PDMS), polyurethane, polyethylene terephthalate, and silicone are widely used as substrates or flexible matrices. These materials can boast high elasticity, wear resistance and easy integration with active substances. Among the active materials, carbon nanotubes (CNT), graphene, conductive polymers, and metallic nanostructures play a key role, providing the formation of stretchable conductive nets inside elastomeric matrices. At the same time, the control of adhesion between the layers, prevention of material degradation and management of filler migration during cyclic deformation remain essential. Here, CNT tubes have an advantage over other active materials, since they have good adhesion to PDMS and silicone due to the formation of strong interfacial bonds [21], and also have a high aspect ratio which enhances the cyclic stability, extensibility, and sensitivity of the related strain gauges. High sensitivity is provided both by the properties of the nanotubes themselves and by the formation of a percolation network capable of stretching and self-healing. The integration of CNT into polymer matrices also allows to achieve high electrical conductivity. The effect of laser radiation on such a network leads to an even greater improvement in both the electrical and mechanical properties of sensors [22].

In the present study, flexible strain gauges were formed on the basis of thin films obtained by sputtering of multiwall CNT dispersions onto silicone substrates. The effect of laser radiation on the internal structure of carbon films was studied. An electrically conductive topology has been obtained using laser lithography. The influence of topology on the electrical characteristics of the strain gauges, tensile stability, temperature stability, and sensitivity to longitudinal deformations is investigated. The possibility of using strain gauges as flexible wearable electronics for respiratory monitoring has been investigated.

1. Materials and methods of research

Section 1 shows the materials used, technical characteristics of the experiments and testing equipment, method of strain gauges fabrication, as well as parameters of laser processing for modifying the morphology of thin films and the formation of a conductive strain-sensitive topology. The parameters of the studied films structure, electrical and mechanical characteristics are also outlined.

1.1. Materials used

Thin carbon films were obtained by deposition of homogeneous dispersions. To fabricate the dispersions, carboxylated carbon nanotubes (CCNT) having $0.1-1.0$ mmol/g of COOH groups and an outer diameter of no more than 50 nm were used. A mixture of ethanol and distilled water was taken as a solvent.

Two-component silicone on a platinum catalyst, Shore hardness 00-10 A, dynamic viscosity 140 Pa·s, Young's modulus at 100 % elongation 0.06 MPa, Shore factor 1.04 g/cm^3, operating temperature range from 19 °C to 232 °C was used for the fabrication of flexible substrates. Liquid silicone was poured into rectangular molds with dimensions of 24×29 mm, printed on an 3D-printer. The silicone mixture was previously placed in a vacuum chamber to remove air bubbles.

1.2. Fabrication of dispersed media made of CNT

To obtain the dispersed media, distilled water and ethanol were mixed in the ratio of 2 : 1, and CCNT were mixed at a concentration of 0.1 mg/ml. The process of dispersing of CCNT in a mixture of distilled water and ethanol included: 1) homogenization with the use of immersive ultrasonic probe during 35 min at a power of 150 W/cm^2; 2) treatment in the ultrasonic bath at a power of 80 W during 15 min.

1.3. Formation of thin films for the flexible strain gauges

Thin films were obtained by deposition of dispersions onto silicone substrates via sputtering method. The sputtering unit included a three-axis positioning system, on the rail and carriage of which the dispenser was fixed. Sputtering was carried out by creating periodic pressure in the dispenser using a compressor when pressing the dispenser button with a bar mounted on the positioning system rack. The amount of dispersion sputtered and, accordingly, the thickness of CNT layer on the substrate depended on the pressure, nozzle diameter and spray intensity. The average dispersion consumption per sample was 15 ml. The silicone substrate was placed on a heating table at a temperature of $100\,^\circ\mathrm{C}-120\,^\circ\mathrm{C}$. This is necessary for the uniform deposition of small droplets of dispersion on the substrate and faster drying of the layers during spraying. The trajectory of the dispenser was set using a software. After the required number of dispersion layers were applied, the resulting CNT film was dried in a dry-air thermostat at a temperature of 100 °C for 1 h.

1.4. Laser processing of carbon films

A ytterbium pulsed fiber laser with a wavelength of 1064 nm, a pulse duration of 100 ns, a spot diameter of 35 μm, and a pulse repetition frequency of 30 kHz was used for laser processing of films. The laser beam travel speed was 500 mm/s. The average radiation power increased sequentially until it was 2 W. The samples were placed in a vacuum chamber, the air from which was pumped out with argon. The average thickness of the irradiated films was 6 μm.

1.5. Study of electrical characteristics

The resistance of the obtained films before and after laser irradiation was studied by a four-probe method using copper-phosphorus alloy probes with a gold coating located at the corners of a square with an inter-probe spacing of 2 mm. The volt-ampere characteristics (VAC) of films at rest and in the stretched state were also obtained using a two-probe method with the help of Summit 12000B-AP semi-automatic probe station and a voltage generator in the supply voltage range from 0.7 to 5 V. The limitation current at voltage of 0.7 and 1 V made 1 μA, at 2 V$-$10 μA, at 5 V$-$100 μA. The carbon films were placed on a polycor

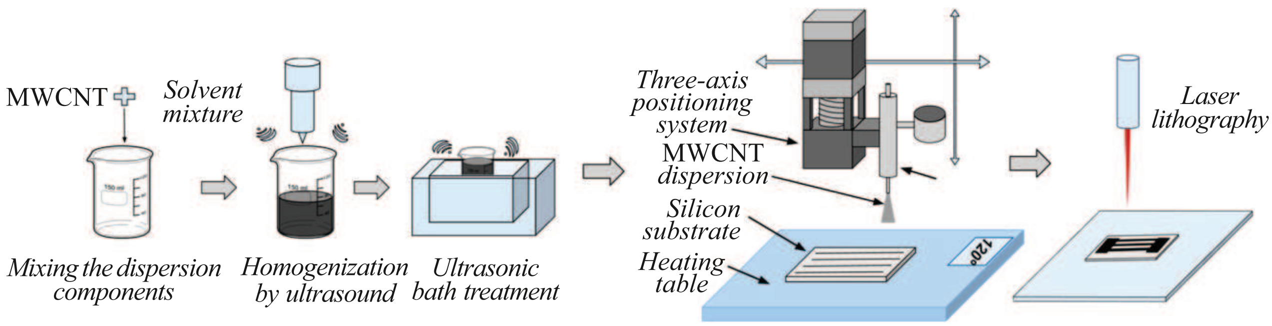

Figure 1. The scheme of forming thin films for flexible strain gauges.

substrate to avoid touching the probes of the metal substrate of the setup.

1.6. Laser lithography for topology formation

Laser lithography was carried out using an ytterbium pulsed fiber laser with a wavelength of 1064 nm, a pulse duration of 100 ns and a frequency of 30 kHz with an average radiation power of 0.887W. The laser beam was focused using lenses to achieve a small spot size on the sample surface. The spot diameter was $\sim 35\,\mu$m, the beam travel speed was 500 mm/s. Before laser processing, the samples consisted of homogeneous layers of CNT on a silicone substrate. The laser processing of surface resulted in formation of a topology in the form of parallel lines of electrically conductive material converging into contact pads located at the two ends of the substrate. Thus, a strain-sensitive electrically conductive topology was formed, which is a CNT structure with a specific pattern. The width of the electrically conductive topology lines was 0.7 mm, the inter-lines spacing was 0.7 mm, the length of the lines was 15 mm, the contact pads were 5×5 mm in size. Thus, the full cycle of fabricating thin carbon films included the steps shown in Fig. 1.

1.7. Investigation of the effect of temperature and stretching on the electrical characteristics of sensors

In this study, the sensors were gradually heated using the thermal system of Summit 12000B-AP probe station. Carbon films with a given topology and without a specific topology were placed on a heated plate, and probes were attached from both sides along the edges of the films. The films were heated up to 100 °C with a step of 5 °C, the volt-ampere characteristics for each temperature range were obtained using the parametric analyzer Keysight B2900. Based on the obtained VAC, the film resistance was calculated for each temperature range. The temperature coefficient of resistance was found using the formula

$$\lambda = \frac{1}{R} \cdot \frac{\Delta R}{\Delta T}, \tag{1}$$

where R — initial resistance at a certain temperature, ΔR — resistance variation when the temperature changes by ΔT.

The strain gauges were formed by attaching carbon wires to a conductive carbon film layer using a mixture of multi-wall CNT (MWCNT) and silicone with a concentration of MWCNT 3 mass % and subsequent application of a protective polymer layer. The setup for studying the strain gauge resistance versus stretching and for measuring the sensitivity coefficient included a dynamometer, a vise to hold the sensor ends, and a stepper motor for gradual stretching and compression that was controlled using a dedicated software.

The sensitivity coefficient was found as follows

$$GF_l = \frac{\Delta R}{R_0} \cdot \frac{1}{\varepsilon}, \tag{2}$$

where R_0 — initial sensor resistance, ΔR — absolute change of resistance when stretched to a value of ε.

1.8. Examination of the internal structure of carbon films

The morphological features of the conductive carbon films obtained by sputtering method were studied using FEI Helios G4 scanning electron microscope (SEM). The accelerating voltage was 5 kV, and the electronic probe current —50 pA. Vacuum chamber pressure was $3.9 \cdot 10^{-4}$ Pa. Three areas were examined: without laser processing and after laser processing with a power of 0.035W and with a power of 0.7W.

2. Results and discussion

Section 2 sheds light on findings from the study of laser radiation effect on electrical and structural properties of thin CNT films, the film topology effect on electromechanical characteristics of strain gauges, research of temperature stability, sensor operability, and their potential use in the respiratory monitoring systems.

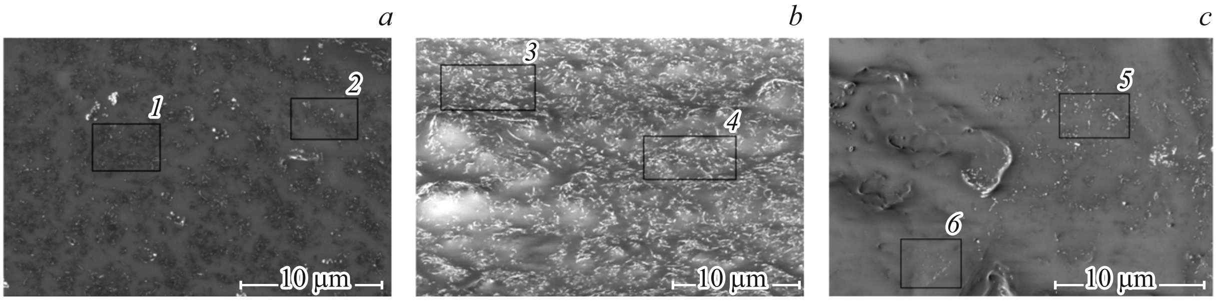

Figure 2. SEM images of carbon films before laser exposure (*a*), after exposure to a laser of 0.035 W (*b*) and after exposure to a laser of 0.07 W (*c*).

2.1. Morphology of carbon films

The carbon layer exposure to laser radiation is an effective method for controlling the functional properties of composite materials, allowing the formation of elements with increased stability and improved compatibility for their integration into electronic circuits. Within the present study, the samples were divided into separate sectors to systematically study the effect of laser radiation parameters on the morphology and structure of thin carbon films. Each sector was exposed to laser radiation with a varying average power of 0.035, 0.07, 0.14, 0.27, 0.54, 1.05 and 2 W. The thickness of the examined carbon coatings measured by optical profilometry, averaged 6 μm. The results of laser modification, including changes in the surface relief and morphology of the carbon layer, were analyzed using scanning electron microscopy (SEM), the results of which are shown in Fig. 2.

It was found that laser exposure led to an increase in the uniformity of CNT distribution in the polymer matrix and a decrease in their size. Fig. 2, *a* shows by digits *1* and *2* the symbols of CNT agglomeratiin areas, Fig. 2, *b* shows by digits *3, 4* the areas of CNT net discharge. In Fig. 2, *c*, in the rectangular areas numbered *5, 6*, there is a noticeable decrease in CNT lengths and partial ablation of silicone matrix nanotubes. According to SEM data, the average length of CNT before laser processing was in the region of 530–790 nm, while after laser exposure 0.035 W this index declined to 270 nm (Fig. 3).

The change in CNT size after laser irradiation is caused by several physical processes. Firstly, this phenomenon is associated with laser ablation, when the pulse energy knocks carbon atoms off the MWCNT surface, which leads to a lower wall thickness and overall diameter without completely destroying the structure of the nanotube. Secondly, the absorption of CNT laser energy leads to a local heating, which causes the rupture of C–C bonds and the introduction of internal defects [24]. MWCNT defects could serve as binding sites for nanotubes in an electrically conductive ordered network, which also affected the electrical conductivity of thin films.

After laser irradiation, the separation of large agglomerates into smaller ones was observed (Fig. 2, *b*), which contributed to a decrease in hysteresis during deformation of carbon films. This effect is explained by lower probability of accidental contacts between nanotubes in a sparse network compared with films containing a significant amount of agglomerates. As a result, the hysteresis of electrical resistance for non-irradiated films reached 12 %, whereas for laser-modified samples this parameter did not exceed 6 % on average.

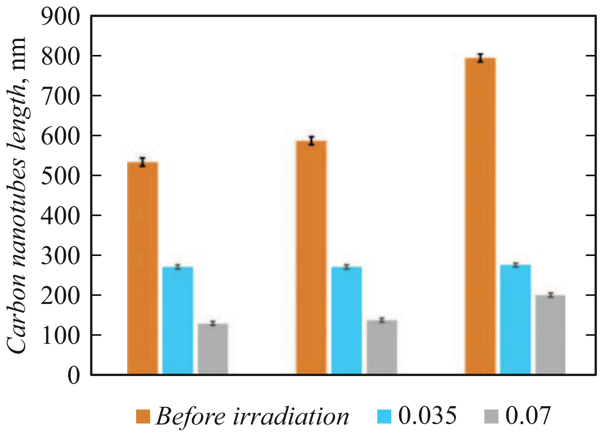

Figure 3. Lengths of CNT before and after laser exposure.

Along with that, a twofold increase in the electrical conductivity of the treated samples was registered. One of the possible reasons is partial ablation of the silicone matrix under thermal radiation effect, due to the presence of residual oxygen in the argon atmosphere. Despite the decrease in the surface concentration of MWCNT, higher conductivity indicates the formation of new covalent bonds between the nanotubes. It should be noted that the use of laser radiation with a power exceeding 0.07 W resulted in the resistance growth by more than 10 times, as well as in the excessive reduction of the nanotubes sizes.

2.2. Carbon films with the specified topology

The change in the topology of the active material of strain gauges is known to lead to a change in both their electrical and strain gauge properties. The formation of

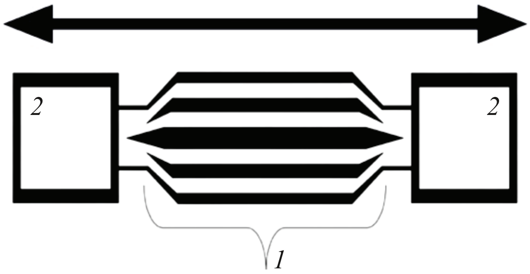

Figure 4. Carbon film topology pattern: *1* — stretching area, *2* — contact pads for connection of electric wires.

topologies can increase the sensitivity of strain gauges to deformation when the number of stress concentrators in the active material becomes higher [25]. In this study, the topology for carbon films (Fig. 4) was developed in order to increase sensitivity to longitudinal deformations and reduce the effect of transverse deformations on changes in the gauge resistance.

The results of measuring the VAC of carbon films using the two-probe method are shown in Fig. 5. The obtained VAC demonstrated a linear dependence of current on voltage, which persisted up to a value of 7 V. For the films without a given topology, a similar linear dependence was observed only up to 5 V. The linear nature of VAC was also maintained under conditions of mechanical stretching of the samples, while the hysteresis value did not exceed 3 % [26]. For the films without a given topology, the preservation of this stability during deformation was not observed. A comparative analysis of the graphs in Fig. 5 shows that the films without a given topology have the deviation from the linear dependence with a growing voltage more pronounced compared to the films with a given topology.

The results of measuring the resistivity of the samples before and after topology formation are presented in the table below. The resistivity value for films with topology was calculated based on the values for each pair of lines, which were considered as parallel resistors.

It was revealed that carbon films with a given topology had an average of 20 times lower resistivity than films without a given topology. However, such a change is rather caused by a significant decrease in the thickness of the conductive paths.

Average resistivity values of carbon films

Type of carbon film	Electrical resistivity, Ω·cm
Without the given topology	6 ± 2
With a given topology	0.3 ± 0.1

2.3. Mechanical characteristics of flexible strain gauges

The formation of the topology also impacted the mechanical characteristics of the thin film sensors. Mechanical characteristics of the developed flexible strain gauges were tested using a setup including a three-axis positioning system with a stepper motor, the trajectory of which was set using a dedicated software. The sample was mounted on a tripod at the base of the positioning system using two fasteners. The samples were moved with a rate of 10 mm/s, the length by which the sample was stretched was 25 mm, which corresponds to 100 % stretching of the sensor. The total size of the strain gauge was 5×25 mm, the size of the topological pattern was — 4.5×24 mm, the length of the electrically conductive topology lines was 18 mm, thickness — 0.9 mm. Fig. 6, *a* illustrates that the curve of the relative change in resistance versus the strain gauge elongation without a given topology has a piecewise linear form, however, the systematic error for the relative change in resistance of a sensor without a given topology is greater than with a given topology (Fig. 6, *b*) and was $2-4$ kΩ, while the error for the strain gauges with topology was $0.6-0.7$ kΩ. The dependence of the relative change in resistance on the elongation of the strain gauges with a given topology has a form close to a linear function with an elongation exceeding 40 %.

In the area of a 35 % stretching, the curve has a piecewise linear form (Fig. 6, *c, d*), which is an important factor in the development of flexible strain gauges, since they shall register the movements of both small and large amplitude. As for the mechanical strength and modulus of elasticity, the change in these parameters after the formation of the topology was minimal. When studying the mechanical characteristics, the initial length between the fasteners was 20 mm, the initial thickness was 0.67mm. The maximum elongation of the strain gauge without a given topology was 300 %, while the tensile strength calculated according to the experimental results was (6.1 ± 0.5) MPa, the modulus of elasticity was (0.14 ± 0.01) kPa, which evidenced the high softness of the material. In the case of the strain gauges with a given topology, the strength and elasticity parameters remained close to the parameters of the strain gauges without a given topology: ultimate strength — (6.1 ± 0.4) MPa, Young's modulus — (0.13 ± 0.01) kPa.

In the area of a 35 % stretching, the curve has a piecewise linear form (Fig. 6, *c, d*), which is an important factor in the development of flexible strain gauges, since they shall register the movements of both small and large amplitude.

As for the mechanical strength and modulus of elasticity, the change in these parameters after the formation of the topology was minimal. When studying the mechanical characteristics, the initial length between the fasteners was 20 mm, the initial thickness was 0.67 mm. The maximum elongation of the strain gauge without a given topology was 300 %, while the tensile strength calculated according to the experimental results was $((6.1 \pm 0.5))$ MPa, the modulus of elasticity was (0.14 ± 0.01) kPa, which evidenced the high softness of the material. In the case of the strain gauges with a given topology, the strength and elasticity

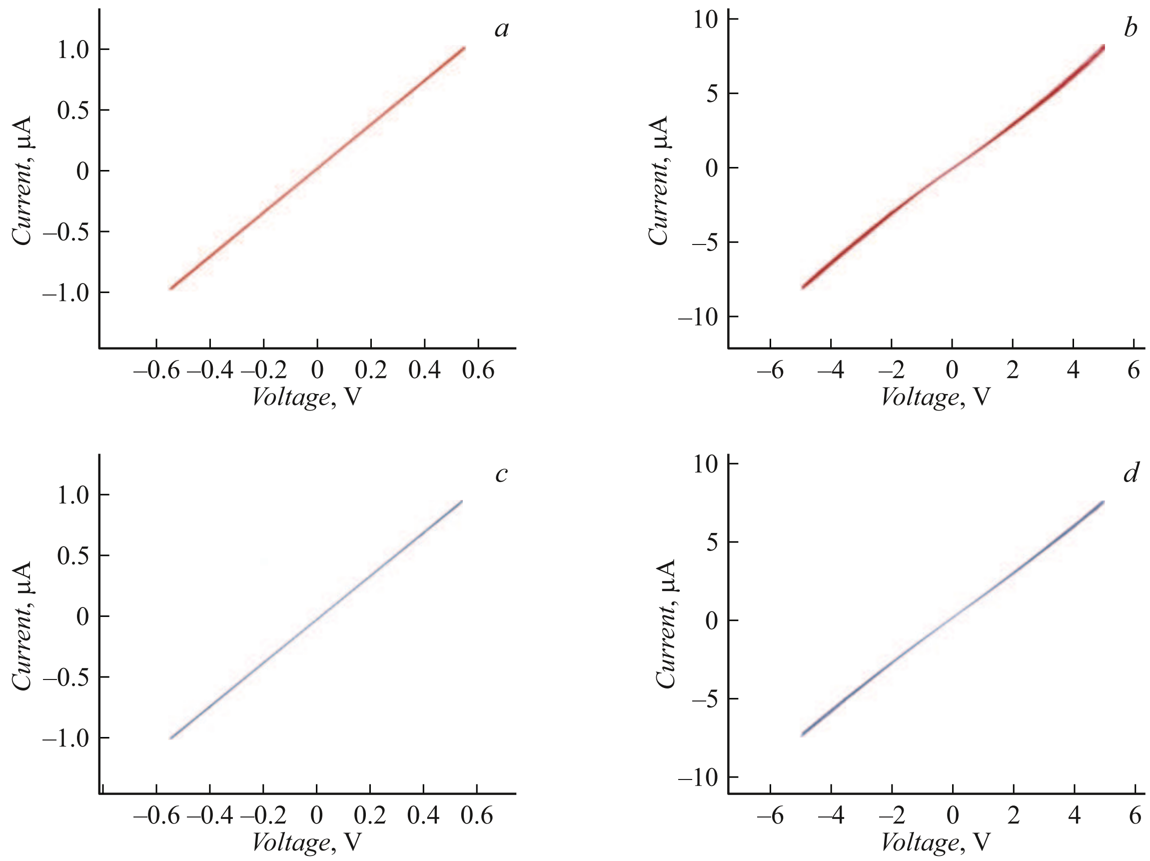

Figure 5. Volt-ampere characteristics with the generator voltage of 0.7 and 5 V respectively, for the films without specified topology (a, b) and films with a given topology (c, d).

parameters remained close to the parameters of the strain gauges without a given topology: ultimate strength — (6.1 ± 0.4) MPa, — (0.13 ± 0.01) kPa.

The formation of topology on carbon films significantly impacted the sensitivity of flexible gauges to elongation strain. Calculated by the formula (2) the sensitivity coefficient was (110 ± 5), while the sensitivity coefficient of the strain gauges without a given topology was about (24 ± 3). The increase in sensitivity is due to the fact that after laser lithography, the electrically conductive strain-sensitive pathways were separated, which led to a lower number of random bonds between CNT that occured during deformation. In addition, the developed type of topology is characterized by the presence of a dedicated stretch area and isolated contact pads. This design solution makes it possible to purposefully localize a mechanical deformation in a given area, which raises the predictability and stability of the electrophysical characteristics of the strain gauges. The presence of separate contact pads minimizes the impact of rigidity of electrical wires and external connections on the working element, ensuring a reliable electrical connection and reducing the risk of damage to the sensitive area during installation.

The strain sensitivity of thin-film sensors varies greatly according to literature. It depends on the method of sensor formation, the thickness of the active layers, the choice of materials, and the topology of composites. Thus, if a network topology is formed on the film made of graphene nanosheets, the sensitivity coefficient GF_l was 38, in case of a „dog bone“ topology— it was 41, in case of a hierarchy structure of „dog bone“ type— 60, with the coefficient error below 10 % [27]. In this study, polyethylene terephthalate was used as a flexible substrate. As can be seen, the formation of topologies affected the sensitivity of the strain gauges, and the increase in sensitivity was associated with a higher number of mechanical stress concentrators in the topologies. The strain-sensitivity of gauges made of bent graphene nanoplates (GNP) on PDMS substrate was about 0.55 [28]. Thin strain-sensitive films can also be obtained by etching graphene on nickel or copper substrates. This method makes it possible to achieve the smallest film thickness, however, the highest value of the sensitivity coefficient GF_l was 6.1 [29]. Low sensitivity of the GNP thin-film strain gauges is often explained by a slight change in the conductive network during deformation, when the distances between the nanoplastics and the contacts between them do not undergo significant shifts. Unlike metal strain gages with $GF_l \approx 2$, where resistance changes due to the piezoresistive effect, the tunneling mechanism dominates in graphene structures, but with insufficient orientation or dense packing

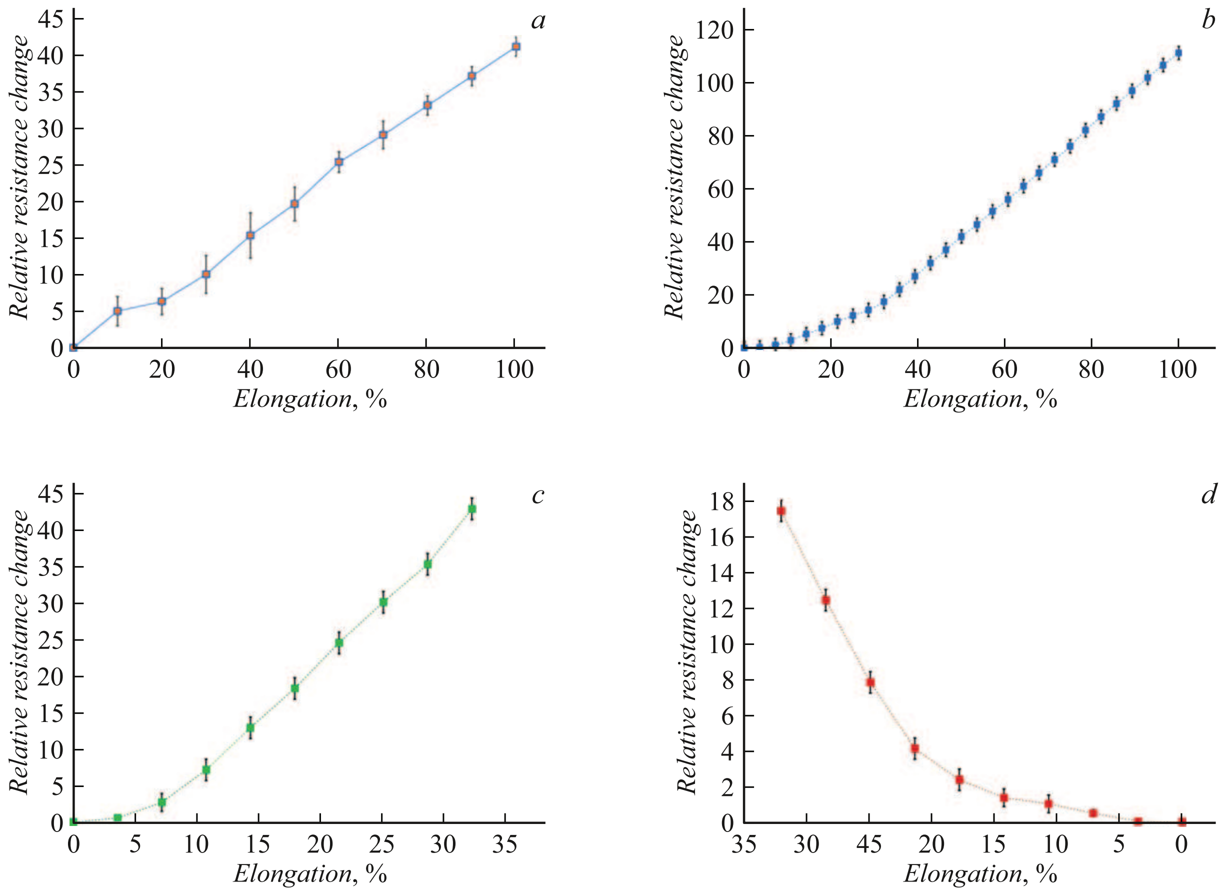

Figure 6. Change of resisitivity when stretched by 100 % for the strain gauges without given topology (a) and with a given topology (b), when the gauges with a given topology are stretched up to 35 % (c) and relaxed (d).

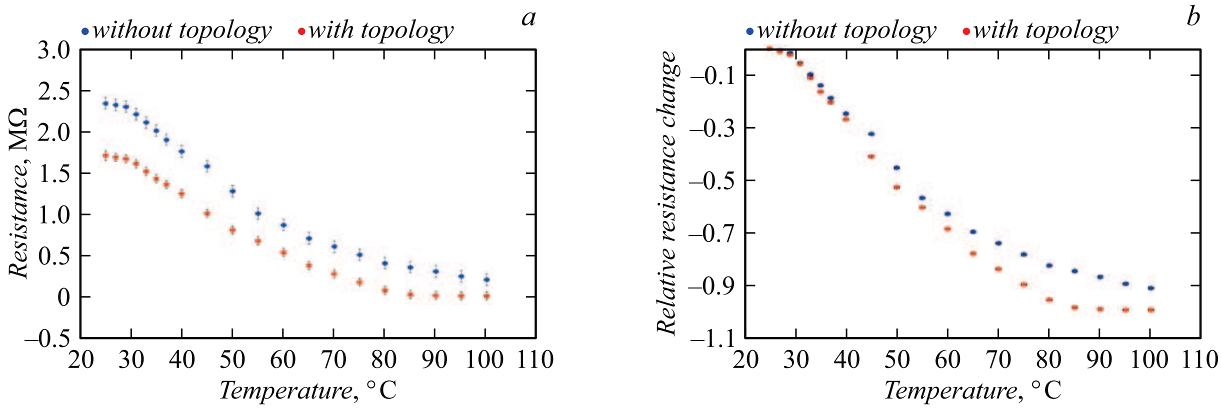

Figure 7. Variation of the strain gauges resistance during heating (a) and relative resistance variation versus temperature (b).

of layers, the tunneling effect is weakly manifested in the range of small deformations. In this case, the change in length and geometry during deformation causes only a linear, rather than an exponential, increase in resistance [30]. In CNT-based strain gauges, piezorestivity also occurs due to the tunneling effect, however, CNT have a high aspect ratio resulting in higher strain sensitivity of the materials made of them. For example, strain gauges made by pressing MWCNT films onto a thermoplastic polyurethane substrate had GF_l of approximately 46 with an elongation of 8.7 % [31]. With a maximum elongation of 300,%, leading to material rupture, the coefficient reached 450. In turn, strain gages based on hybrid nanomaterial film from MWCNT and GNP deposited on a polyimide substrate by sputtering method demonstrated sensitivity of about 24 [32]. Moreover, it was found that this parameter depends on the volume of the sputtered dispersion, and hence on the thickness of the film.

Thus, the new MWCNT-based thin-film strain gauges with a conductive topology outpace most of the existing solutions in terms of strain sensitivity.

2.4. Temperature effect on the gauges operability

Resistance to temperature variations is a critical feature of flexible sensors, since temperature fluctuations induce parasitic changes in electrical resistance that mask the useful signal from mechanical deformation. This undesirable reaction, known as temperature error, can significantly reduce the accuracy and reliability of measurements in unstable thermal environments. Overcoming this effect is achieved through the use of dedicated circuits, such as a Wheatstone bridge circuit with a passive or active temperature compensator, as well as through the development of composite materials with a low or predictable temperature coefficient of resistance.

In the development of flexible sensors, the effect of temperature on the resistance of strain gauges without a given topology and with a given topology, as well as the possibility of temperature affecting the operability, was investigated in this work. The dependencies shown in Fig. 7 were plotted.

The resistance was found to decrease with the temperature rise. Moreover, the presence of a topology makes practically no difference in the sensors' response to heating, which is reflected in Fig. 7, *a*. However, it can be seen in Fig. 7, *b* that sensors with a given topology are more sensitive to heat at temperatures above $50\,^\circ$C. This may be due to the lower volume concentration of CNTs in the silicone matrix, as part of the nanotubes evaporated during laser ablation. The temperature coefficients also indicate this: the temperature coefficient of the strain gauges in the temperature range $25\,^\circ\mathrm{C}-45^\circ$ with a given topology was $-20 \cdot 10^{-3}\,\mathrm{K}^{-1}$, while the coefficient for sensors without a given topology was $-16 \cdot 10^{-3}\,\mathrm{K}^{-1}$. The described temperature range was chosen based on the assumption that when worn on the human body, the heating of the sensors will not exceed $45\,^\circ$C.

In addition, there was a need to assess the effect of temperature on the operability of flexible strain gauges. To do this, using mathematical modeling methods based on the dependence of resistance on elongation and resistance on temperature, the distribution of resistance variation during interaction of these factors was obtained (Fig. 8). Fig. 8 illustrates relative temperature variation along X axis, relative stretching — along Y axis. The Z axis displays the corresponding value of the relative electrical resistance. The graph shows that with an increase in both temperature and stretching, there is an increase in sensor resistance. The surface has a monotonously increasing character, especially when both variables are simultaneously increasing. This indicates the combined effect of thermal and mechanical factors on the conductivity of the material. The color scale located on the left corresponds to the resistance values and illustrates the gradient of change from purple (small change in resistance) to yellow (large change in resistance), emphasizing the sensitivity of the strain gauges to the temperature and deformation effects.

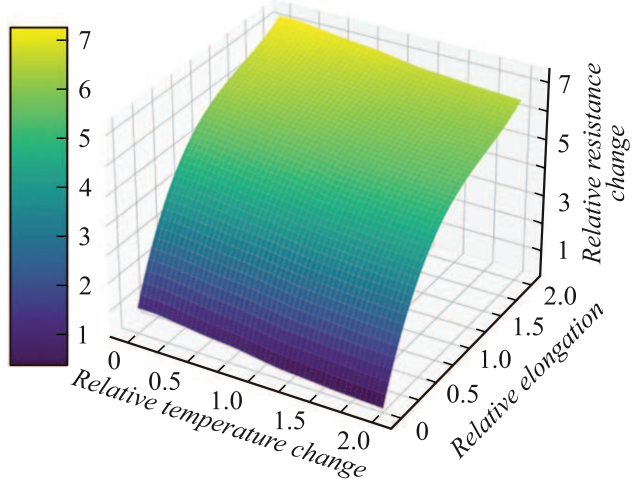

Figure 8. Interdependence of strain gauges' resistance on temperature and elongation.

However, the slope of the graph lines in XZ plane is not noticeable in comparison with the curvature of the graph in YZ plane. In addition, heating the sensor by 200 % corresponds to stretching the sensor by only 20 %. These observations indicate that the temperature contribution to the change in the strain gauge resistance is not significant compared to the effect of stretching. Therefore, heating during operation will not make major changes to the operation of the presented flexible strain gauges.

2.5. Respiratory monitoring

Registration of respiratory activity is an essential element of diagnosis and monitoring in various pathologies. This need arises not only in diseases of the respiratory system, such as COPD, bronchial asthma, but also in disorders of neurological origin, when respiratory centers or pathways are affected, for example, sleep apnea, the effects of stroke, neuromuscular diseases. Clinical manifestations of respiratory failure can range from tachypnea, rapid breathing, and shortness of breath to complete transient respiratory arrest and apnea, which are directly life-threatening. In this regard, continuous monitoring of respiratory activity is a crucial task in clinical practice. Traditional inpatient monitoring systems limit patient mobility, but the use of modern flexible strain gauges opens up new possibilities for long-term and continuous monitoring of breathing in outpatient conditions. These devices, being non-invasive, are highly sensitive and allow registering the chest or diaphragm behaviour, which ensures the collection of objective data on the nature and rhythm of breathing in real time outside the hospital.

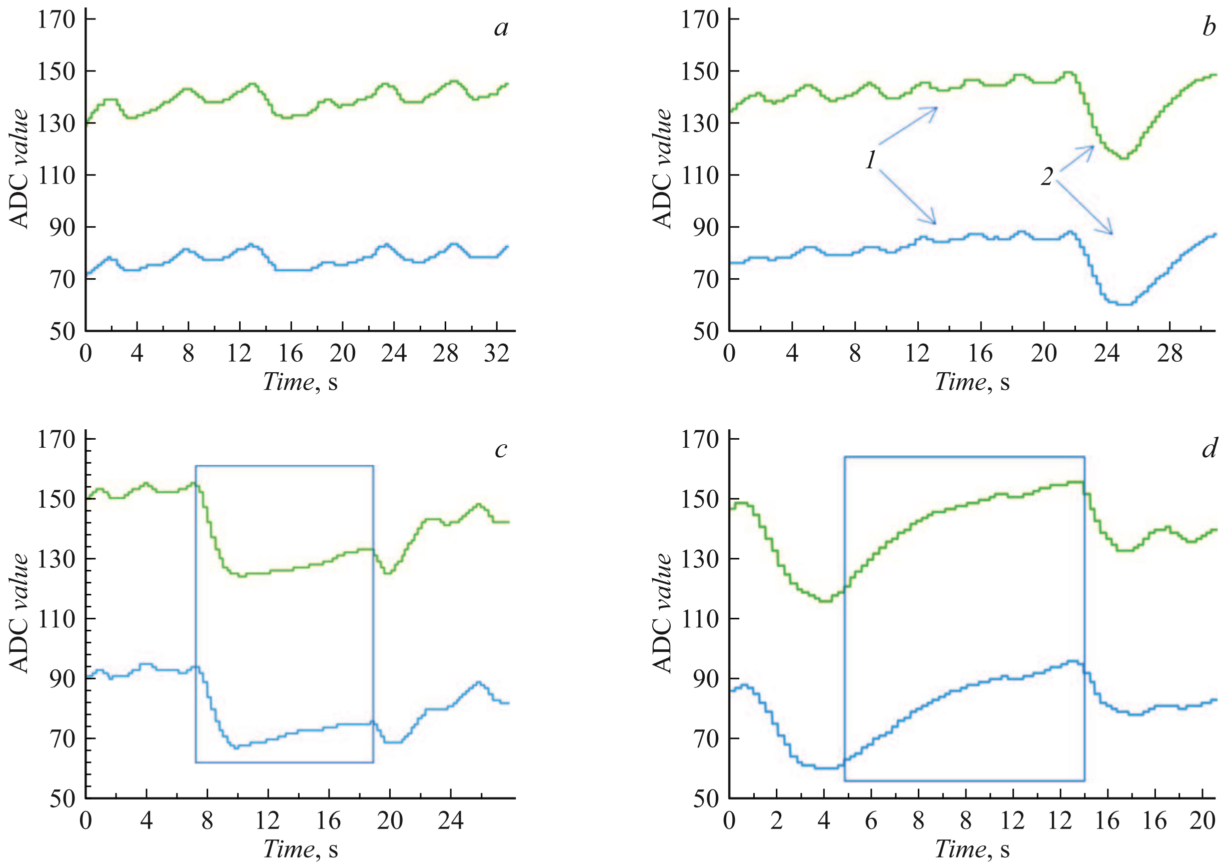

Figure 9. The signal from two strain gauges with a given topology at different initial resistance during normal breathing rhythm (*a*), rapid breathing frequency and abrupt inspiration (*b*): indicated by the numbers *1* and *2*, respectively. The area of the signal when stopping breathing on breathing in (*c*) and breathing out (*d*).

To investigate the possibility of respiratory monitoring, the developed strain gauges were connected to an electronic unit that processed changes in sensor resistance using an analog-to-digital converter (ADC), noise filtering, and signal transmission via Bluetooth to a PC, where real-time signal graphs were displayed. The numerical values of the signal were recorded in a csv file. Flexible sensors were attached to an elastic textile strap, which was fixed in the area of the lower aperture of the chest. The reaction of strain gauges to breath holding during breathing-in and breathing-out, during slow deep breathing and normal breathing rhythm was studied (Fig. 9).

For rapid breathing with a sharp intake of breath, the recording interval of the signal was 30 s, for normal — 32 s (Fig. 9, *a, b*).

From 22 to 28 s as seen in Fig. 9, *b* an abrupt deep breathing-in is observed. For rapid breathing, the average frequency was about 0.3 Hz, for normal breathing, the average respiratory rate was 0.5 Hz, but the average difference in the amplitudes of ADC values for the two types of breathing was 3 ADC values for both sensors. The total time of signal measurement for the breath holding on breathing-in was 27 s, for the breath holding on breathing-out — 20 s (Fig. 9, *c, d*). The change in the ADC signal in a positive or negative direction directly depended on the direction of breathing: i.e. stretching or compressing the sensors, respectively. Rectangular frames in Fig. 9, *c, d* highlight the moments of respiratory failure, which were 11 s on breathing-out and 10 s on breathing-in for both strain gauges. The appearance of a small peak at 19 s (Fig. 9, *c*) is associated with the movement of the operator's body during the experiment. The breathing-in amplitude was 30 of ADC values for the first sensor and 27 for the second; the breathing-out amplitude was 40 of ADC values for the first sensor and 35 for the second.

Conclusion

The conducted studies confirm the possibility of creating flexible strain gauges based on thin CNT films for respiratory monitoring, and also indicate the effectiveness of the method of modifying the strain gauges properties using laser lithography. The formation of an electrically conductive strain-sensitive topology led to a significant increase in the sensitivity coefficient of the sensors at a low hysteresis value. Laser modification of the carbon films surface also contributed to higher electrical conductivity of the material due to the redistribution of CNT network in the silicone matrix.

Within the framework of the study, patterns of mutual influence of stretching and heating of the strain gauges were identified, which confirmed the operability of sensors as flexible wearable electronics devices. The mechanical and electrical characteristics of the sensor material were also determined.

The presented flexible strain gauges showed the ability to register various breathing rhythms, as well as respiratory failure during both breathing-in and breathing-out.

The study was performed using the equipment of the Core Shared Research Facility „Center for Laser Technologies in Medicine“ with the support of the Ministry of Science and Higher Education of Russian Federation (Agreement № 075-15-2025-669 of 05 August 2025)

Funding

The work was performed under the state assignment of the Ministry of Education and Science of Russia (Project FSMR-2024-0003).

Conflict of interest

The authors declare that they have no conflict of interest.

References

[1] H. Yao, T. Sun, J.S. Chiam, M. Tan, K.Y. Ho, Z. Liu, B.C.K. Tee. Adv. Funct. Mater., **31**, 2008650 (2021). DOI: 10.1002/adfm.202008650
[2] Y. Wang, X. Li, S. Fan, X. Feng, K. Cao, Q. Ge, L. Gao, Y. Lu. ACS Appl. Mater. Interfaces, **13**, 8901 (2021). DOI: 10.1021/acsami.0c21086
[3] Y. Kim, A. Chortos, W. Xu, Y. Liu, J.Y. Oh, D. Son, J. Kang, A.M. Foudeh, C. Zhu, Y. Lee, S. Niu, J. Liu, R. Pfattner, Z. Bao, T.-W. Lee. Science, **360**, 998 (2018). DOI: 10.1126/science.aao0098
[4] L. Wang, K.J. Loh, W.-H. Chiang, K. Manna. Nanotechnology, **29**, 105503 (2018). DOI: 10.1088/1361-6528/aaa2d
[5] Y. Chu, J. Zhong, H. Liu, Y. Ma, N. Liu, Y. Song, J. Shao, Z. Shao, Y. Sun, Y. Dong, X. Wang, L. Lin. Adv. Funct. Mater., **28**, 1803413 (2018). DOI: 10.1002/adfm.201803413
[6] S.J. Benight, C. Wang, J.B.H. Tok, Z. Bao. Prog. Polym. Sci., **38**, 1961 (2013). DOI: 10.1016/j.progpolymsci.2013.08.001
[7] Z. Ma, W. Shi, K. Yan, L. Pan, G. Yu. Chem. Sci., **10**, 6232 (2019). DOI: 10.1039/C9SC02033K
[8] A.F. Paterson, S. Singh, K.J. Fallon, T. Hodsden, Y. Han, B.C. Schroeder, H. Bronstein, M. Heeney, I. McCulloch, T.D. Anthopoulos. Adv. Mater., **30**, 1801079 (2018). DOI: 10.1002/adma.201801079
[9] A.S. Morozova, A.V. Kuksin, A.Y. Gerasimenko. Biomed Eng., **59**, 131 (2025). DOI: 10.1007/s10527-025-10479-3
[10] S. Xu, Y. Zhang, J. Cho, J. Lee, X. Huang, L. Jia, J.A. Fan, Y. Su, J. Su, H. Zhang, H. Cheng, B. Lu, C. Yu, Ch. Chuang, Tae-il Kim, T. Song, K. Shigeta, S. Kang, C. Dagdeviren, I. Petrov, P.V. Braun, Y. Huang, U. Paik, J.A. Rogers. Nat. Commun., **4**, 1543 (2013). DOI: 10.1038/ncomms2553
[11] J. Zhao, C. Zhang, D. Zou, X. Liu, L. Cai, X. Li, M. Shi. Adv. Mater. Technol., **4**, 1900492 (2019). DOI: 10.1002/admt.201900492
[12] S.C.B. Mannsfeld, B.C.-K. Tee, R.M. Stoltenberg, C.V.H.-H. Chen, S. Barman, B.V.O. Muir, A.N. Sokolov, C. Reese, Z. Bao. Nat. Mater., **9**, 859 (2010). DOI: 10.1038/nmat2834
[13] L. Pan, A. Chortos, G. Yu, Y. Wang, S. Isaacson, R. Allen, Y. Shi, R. Dauskardt, Z. Bao. Nat. Commun., **5**, 3002 (2014). DOI: 10.1038/ncomms4002
[14] M. Amjadi, Y.J. Yoon, I. Park. Nanotechnology, **26**, 375501 (2015). DOI: 10.1088/0957-4484/26/37/375501
[15] J.S. Bergström, M.C. Boyce. Mech. Mater., **33**, 523 (2001). DOI: 10.1016/S0167-6636(01)00068-9
[16] Y.-C. Huang, Y. Liu, C. Ma, H.-C. Cheng, Q. He, H. Wu, C. Wang, C.-Y. Lin, Y. Huang, X. Duan. Nat. Electron., **3**, 59 (2020). DOI: 10.1038/s41928-019-0356-5
[17] B.C.-K. Tee, C. Wang, R. Allen, Z. Bao. Nat. Nanotechnol., **7**, 825 (2012). DOI: 10.1038/nnano.2012.192
[18] H. Kong, Z. Song, W. Li, Y. Bao, D. Qu, Y. Ma, Z. Liu, W. Wang, Z. Wang, D. Han, L. Niu. ACS Nano, **15**, 16218 (2021). DOI: 10.1021/acsnano.1c05028
[19] G. Ge, Y. Lu, X. Qu, W. Zhao, Y. Ren, W. Wang, W. Wang, W. Huang, X. Dong. ACS Nano, **14**, 218 (2020). DOI: 10.1021/acsnano.9b07874
[20] Y.J. Park, B.K. Sharma, S.M. Shinde, M.-S. Kim, B. Jang, J.-H. Kim, J.-H. Ahn. ACS Nano, **13**, 3023 (2019). DOI: 10.1021/acsnano.8b07995
[21] M. Amjadi, Y.J. Yoon, I. Park. Nanotechnology, **26**, 375501 (2015). DOI: 10.1088/0957-4484/26/37/375501
[22] A.M.V. Mohan, V. Rajendran, R.K. Mishra, M. Jayaraman. Nano, **11**, 1875 (2021). DOI: 10.3390/nano11081875
[23] S. Li, Y. Zhang, Y. Wang, K. Xia, Z. Yin, H. Wang, M. Zhang, X. Liang, Y. Lu, M. Zhu, H. Wang, X. Shen, J.A. Fan. Micromachines, **14**, 1106 (2023). DOI: 10.3390/mi14061106
[24] A.Yu. Gerasimenko. Kondensirovannye sredy i mezhfaznye granitsy, **19** 489 (2017) (in Russian). DOI: 10.17308/kcmf.2017.19/227
[25] J. Lee, S. Kim, J. Lee, D. Yang, B.C. Park, S. Ryu, I. Park. Sci. Rep., **12**, 10467 (2022). DOI: 10.1038/s41598-022-13393-w
[26] A.S. Morozova, A.Yu. Gerasimenko. *Materialy nauchno-tekhnicheskoy konferentsii „Mikroelektronika i informatika-2025“*. Collection of articles (Moscow–Zelenograd, 25—26 April 2024, 137, 2025)
[27] L. Wang, W.-H. Chiang, K.J. Loh. Sci. Rep., **12**, 9179 (2022). DOI: 10.1038/s41598-022-13393-w
[28] Y. Wang, R. Yang, Z.W. Shi, L.C. Zhang, D.X. Shi, E. Wang, G.Y. Zhang. ACS Nano, **5**, 3645 (2011). DOI: 10.1021/nn103523t
[29] Y. Lee, S. Bae, H. Jang, S. Jang, S.E. Zhu, S.H. Sim, Y.I. Song, B.H. Hong, J.H. Ahn. Nano Lett., **10**, 490 (2010). DOI: 10.1021/nl903272n
[30] F.S. Irani, A.H. Shafaghi, M.C. Taşdelen, T. Delipınar, C.E. Kaya, G.G. Yapici, M.K. Yapici. Micromachines, **13**, 119 (2022). DOI: 10.3390/mi13010119
[31] P. Slobodian, R. Daňová, R. Olejník, J. Matyáš, L. Münster. Polym. Adv. Technol., **30**, 1891 (2019). DOI: 10.1002/pat.4621
[32] S.-C. Her, Y.-M. Liang. Sensors (Basel), **22**, 5039 (2022). DOI: 10.3390/s22135039

Translated by T.Zorina